

Perspective

Application of First Principles Computations Based on Density Functional Theory (DFT) in Cathode Materials of Sodium-Ion Batteries

Yuqiu Wang ¹, Binkai Yu ¹, Jin Xiao ², Limin Zhou ^{1,*} and Mingzhe Chen ^{1,*} 

¹ School of Energy and Power Engineering, Nanjing University of Science and Technology, Nanjing 210094, China

² School of Science, Hunan University of Technology, Zhuzhou 412007, China

* Correspondence: lmzhou@njust.edu.cn (L.Z.); chenmingzhe@njust.edu.cn (M.C.)

Abstract: Sodium-ion batteries (SIBs) have been widely explored by researchers because of their abundant raw materials, uniform distribution, high-energy density and conductivity, low cost, and high safety. In recent years, theoretical calculations and experimental studies on SIBs have been increasing, and the applications and results of first-principles calculations have aroused extensive interests worldwide. Herein, the authors review the applications of density functional (DFT) theory in cathode materials for SIBs, summarize the applications of DFT in transition-metal oxides/chalcogenides, polyanionic compounds, Prussian blue, and organic cathode materials for SIBs from three aspects: diffusion energy barrier and diffusion path, energy calculation and structure, and electronic structure. The relationship between the structure and performance of the battery material will be comprehensively understood by analyzing the specific working principle of battery material through theoretical calculation and combining with high-precision experimental characterization technologies. Selecting materials with good performance from a large number of electrode materials through theoretical calculation can avoid unnecessary complex experiments and instrument characterizations. With the gradual deepening of research, the DFT calculation will play a greater role in the sodium-ion battery electrode field.

Keywords: sodium-ion batteries; cathode materials; first-principles computations; density functional theory



Citation: Wang, Y.; Yu, B.; Xiao, J.; Zhou, L.; Chen, M. Application of First Principles Computations Based on Density Functional Theory (DFT) in Cathode Materials of Sodium-Ion Batteries. *Batteries* **2023**, *9*, 86. <https://doi.org/10.3390/batteries9020086>

Academic Editor: Carlos Ziebert

Received: 7 December 2022

Revised: 23 January 2023

Accepted: 26 January 2023

Published: 27 January 2023



Copyright: © 2023 by the authors. Licensee MDPI, Basel, Switzerland. This article is an open access article distributed under the terms and conditions of the Creative Commons Attribution (CC BY) license (<https://creativecommons.org/licenses/by/4.0/>).

1. Introduction

As early as the 1970s, sodium-ion batteries (SIB) and lithium-ion batteries (LIB) were investigated almost at the same time. However, due to the excellent characteristics of LIBs and the limitations of research conditions, research on SIBs were developing slowly. In recent years, with the huge demand for renewable energy and the attentions paid to environmental pollution, the research on sodium-ion batteries has returned to people's attention [1–9]. Additionally, because it can alleviate the resource shortage caused by excessive exploitation of LIB raw materials and the limited development of energy storage batteries caused by rising material prices, to a certain extent, it has attracted extensive attentions from researchers all over the world.

The cathode material is an important part of SIBs, which directly determines the battery performance and the upper limit of cell energy density [10–13]. The cathode materials that can be widely used must meet the following requirements. First, the cathode material should have a high-redox potential so that a high-output voltage can be obtained by maintaining the electrodynamic force of the SIBs. At the same time, the embedding and stripping of charged ions have a minor impact on the electrode potential so there will be no excessive voltage fluctuation during the charging and discharging process, which will not bring adverse effects to other electrical devices in the system. Second, the sodium content

of the material is high, and the sodium-ion insertion is reversible. This is a prerequisite for high capacity. Third, as the Na^+ diffusion coefficient is higher, the Na^+ moves more quickly in the material so the ability to insert and de-insert is stronger. Fourth, in the process of sodium-ion inserting/deinterlacing, the structure of the positive electrode material should not change significantly to ensure the long-term stability of the battery. Fifth, it has good conductivity to ensure the sodium-ion battery can be charged and discharged with a high current. Sixth, the materials are easy to be obtained and have good processing performance.

To obtain the ideal cathode material, it is especially important to better understand its working mechanism. Theoretical calculation and simulation can help us to further understand the nature of electrode materials. Analyzing the energy storage mechanism of battery materials by theoretical calculation can analyze the electrochemical reaction kinetic from the nanometer scale, and the relationship between structure and performance can often be well explained by combining high-precision experimental characterization techniques. Density functional theory is widely used as a representative [14–17]. At present, the DFT calculation is widely used to estimate the structural stability of battery materials, study the sodium insertion voltage of electrode materials, calculate the diffusion barrier and diffusion path, analyze the electronic structure of battery materials, and simulate the adsorption process of ions or molecules [18–25]. Given the importance and contribution of DFT calculation in the study of SIBs, this perspective summarizes the latest progress in the DFT calculation of SIB cathode materials from transition-metal oxides/chalcogenides, polyanionic compounds, Prussian blue, and organic cathode materials, respectively. This perspective focuses on the key role of the DFT calculation in the development of cathode materials for SIB and guides the further developments of DFT in the field of electrode materials in the future.

2. Principle of DFT Calculation

As long as some basic physical quantities (such as reduced Planck constant, atomic mass, and electronic electric quantity) are used, the physical and chemical properties of materials can be calculated through the Schrodinger Equation (1). Therefore, theoretical calculations based on the Schrodinger equation are generally first-principles calculations

The Schrodinger equation has the following form [26]:

$$i\hbar \frac{\partial}{\partial t} \psi(\mathbf{r}, t) = \hat{H} \psi(\mathbf{r}, t) \quad (1)$$

In the equation, i is an imaginary unit; \hbar represents the reduced Planck constant; $\frac{\partial}{\partial t}$ is the item partial derivative operator; $\psi(\mathbf{r}, t)$ represents the wave function of the system; \hat{H} is the Hamiltonian operator of the system.

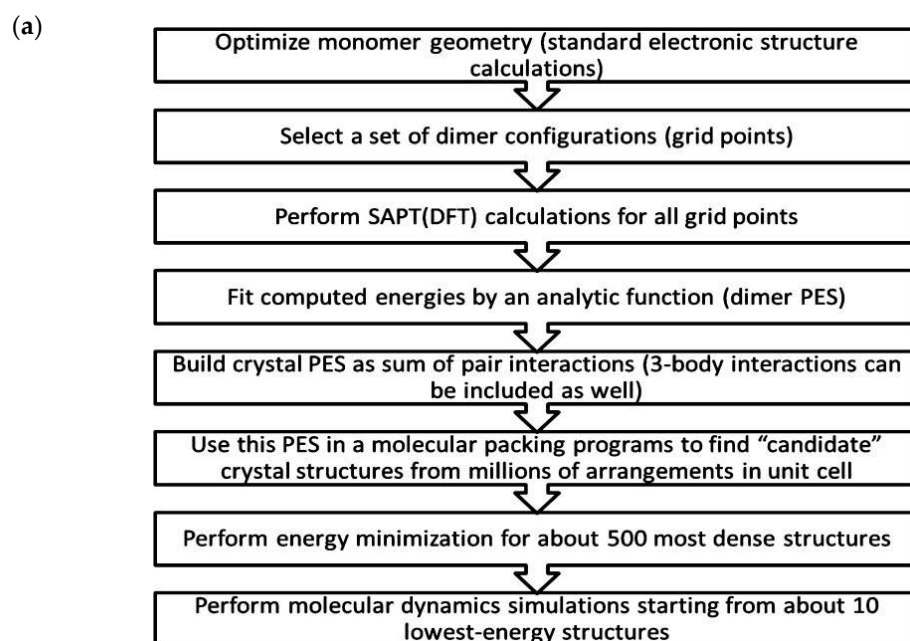
To solve the problem that the equations are difficult to solve due to the multi-body interaction in the first principle calculation, researchers have proposed a series of simplification and approximation methods, among which the DFT is the most widely used [27–33]. The core idea of DFT is not to directly solve the electron wave function of the multi-body interaction system but to link the Hamiltonian with the electron density and express the total energy, E , as the function of electron density. After the Kohn–Sham [34] hypothesis is introduced, the problem of the interaction system was transformed into a non-interaction problem that is easy to separate variables; the process of solving the electron ground state energy was transformed into a self-consistent iterative process of the Kohn–Sham Equation (2). After obtaining a self-consistent convergent charge density, n_0 , the total energy of the system can be obtained (3). The first-principles calculation is widely used in crystallography. For example, the first principles are used to determine the crystal structure. The steps are shown in Figure 1a.

$$\left(-\frac{1}{2} \nabla^2 + v_{\text{ext}}(\vec{\mathbf{r}}) + v_{\text{H}}(\vec{\mathbf{r}}) + v_{\text{xc}}(\vec{\mathbf{r}}) \right) \Phi_i = \varepsilon_i \Phi_i \quad (2)$$

$$E_0 = \sum_i^N \varepsilon_i - \frac{q^2}{2} \int d^3r \int d^3r' \frac{n_0(\vec{r})n_0(\vec{r}')}{|\vec{r} - \vec{r}'|} - \int d^3r v_{xc}(\vec{r})n_0(r) + E_{xc}[n_0] \quad (3)$$

In Equation (2), $v_{\text{ext}}(\vec{r})$ represents external potential, $v_{\text{H}}(\vec{r})$ represents Hartree potential, and $v_{\text{xc}}(\vec{r})$ is exchange-correlation potential. In Equation (3), ε_i represents the eigenvalue of the KS equation.

With the development of DFT, the application of the first principles has been expanded by the combination of many theories, shown in Figure 1b,c.



(b)

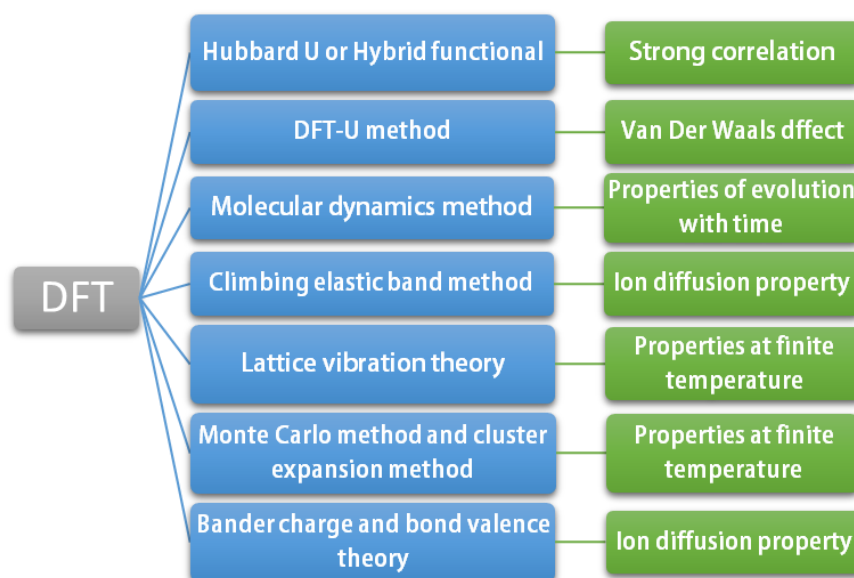


Figure 1. Cont.

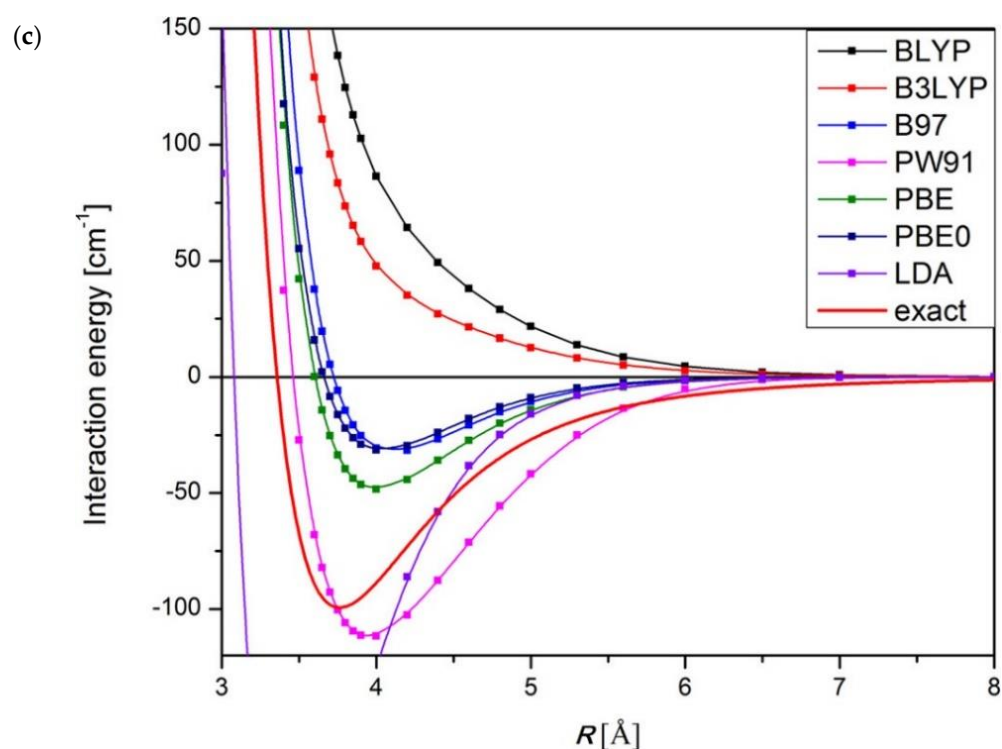


Figure 1. (a) The step of determining crystal structure by the first principles [35]. (b) Density functional theory combined with various theoretical methods. (c) Performance comparison of argon dimer by different DFT methods. The datum curve [36] is accurate to its line width. The acronyms define various DFT methods, for example, see Reference [37]. Reprinted (adapted) with permission from Ref. [35]. Copyright 2014, American Chemical Society.

3. Application of DFT Calculation in Transition-Metal Oxides/Chalcogenides

Transition-metal oxides possess periodic structures, simple preparation methods, and high specific capacity, and high voltage. Transition-metal chalcogenides have the advantages of large interlayer space, fast ion transfer kinetics, and large theoretical capacity. They are the main cathode materials of SIBs. This section introduces the application of the DFT calculation in transition-metal oxides/chalcogenides.

3.1. Energy Calculation and Structural Stability Judgment

For a conventional chemical reaction, in the standard state, the Gibbs free energy expression for the response is as follows [23].

$$G = H - TS \quad (4)$$

$$H = E + PV \quad (5)$$

Here, G , H , S , E , T , P , and V represent Gibbs free energy, enthalpy, entropy, internal energy, temperature, pressure, and volume, respectively. For the cell system with constant volume at low temperature and normal pressure, the Gibbs free energy of the reaction is equivalent to the internal energy change before and after the reaction. Based on this, the specific capacity of electrode materials in the battery and the mass/volume energy density of the battery can be obtained by calculating the internal energy change of the reaction. We can calculate the voltage of the electrode to metal sodium by calculating the Gibbs free energy released by the entire electrochemical system when transferring unit electrons, and we also can judge the stability of the electrode structure by calculating the cohesive energy, formation energy, free energy, etc.

Generally, there are many sodium vacancies in the electrode lattice of the stripped or embedded state, and there are many different configurations. To get the most stable configuration, we need to calculate and compare the energy of all possible configurations. Alexandra J. Toumar et al. [38] calculated the sodium insertion curve and sodium content configuration energy diagram of Na_xCrO_2 materials, shown in Figure 2a, and other O3 type layered oxides by DFT and cluster expansion method and analyzed the potential sequence corresponding to the redox electric pairs of transition metals in O3 type layered oxides by calculating the energy of thermo dynamic stable configurations of different layered oxides: $\text{Ti}^{4+}/\text{Ti}^{3+} < \text{V}^{4+}/\text{V}^{3+} < \text{Mn}^{4+}/\text{Mn}^{3+} < \text{Co}^{4+}/\text{Co}^{3+} < \text{Ni}^{4+}/\text{Ni}^{3+} < \text{Cr}^{4+}/\text{Cr}^{3+} < \text{Fe}^{4+}/\text{Fe}^{3+}$, shown in Figure 2b.

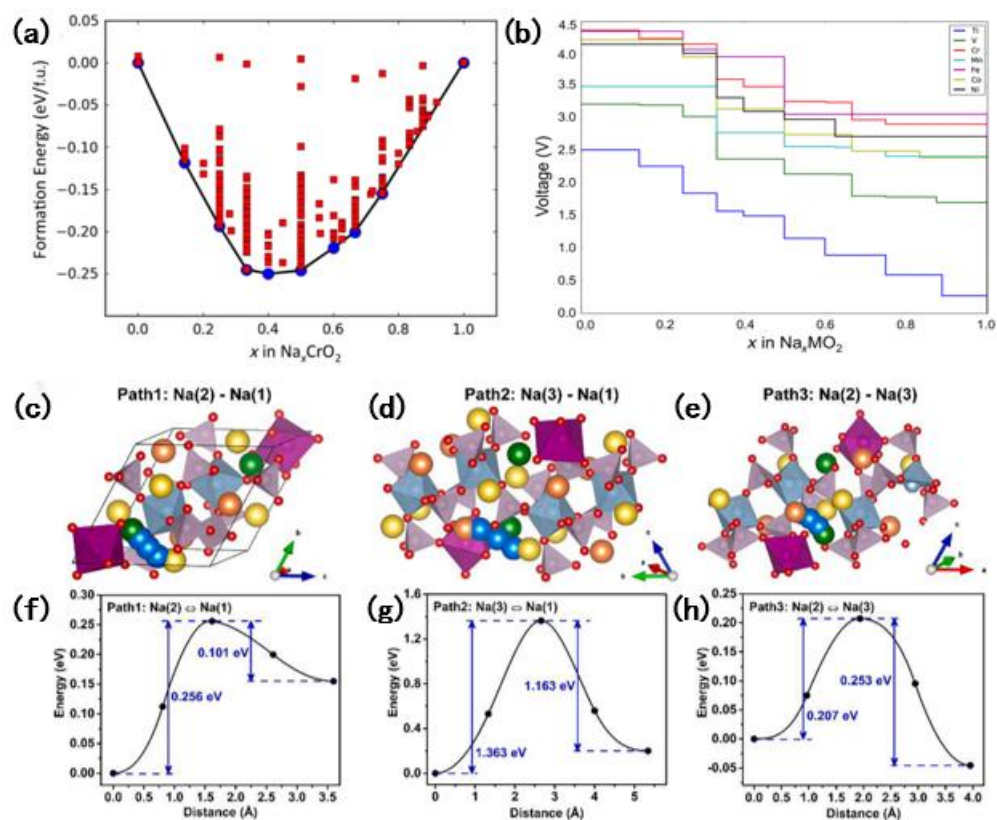


Figure 2. (a) Sodium content configuration energy diagram of Na_xCrO_2 materials. (b) Calculation curve of O3 type Na_xMO_2 ($M = \text{Ti}, \text{V}, \text{Mn}, \text{Co}, \text{Ni}, \text{Cr}, \text{Fe}$) sodium-embedding voltage. Reprinted (figure) with permission from Ref. [38]. Copyright 2015, American Physical Society. Diffusion paths of sodium in $\text{Na}_4\text{MnAl}(\text{PO}_4)_3$ and DFT calculation results of corresponding energy barrier of (c,f) Path1: Na(2)–Na(1), (d,g) Path2: Na(3)–Na(1) and (e,h) Path3: Na(2)–Na(3). Reprinted (adapted) with permission from Ref. [39]. Copyright 2021, Elsevier.

The high average metal oxidation state in the synthesis of layered transition metal oxide, Na_xMnO_2 , means the P2 alloy needs to introduce high-valence cations, which limits the performance of the cathode. Matteo Bianchini et al. [40] studied the possibility of P2 cathode containing only electrochemically active Ni and Co cations by first principles calculation and experiment. The results show when $x = 0.66, 0.75$ and $0 \leq y \leq 0.33$, the P2 $\text{Na}_x\text{Ni}_y\text{Co}_{1-y}\text{O}_2$ material has thermodynamic stability or metastable state at the typical P2 synthesis temperature (≈ 1000 K) and can successfully synthesize new P2 compounds with $\text{Ni}_{3+/4+}$ and $\text{Co}^{3+/4+}$. This work expanded the current knowledge of P2 materials.

In the first charge discharge cycle, $\text{Na}_{0.75}[\text{Li}_{0.25}\text{Mn}_{0.75}]\text{O}_2$ with honeycomb superstructure has obvious voltage loss compared with $\text{Na}_{0.6}[\text{Li}_{0.2}\text{Mn}_{0.8}]\text{O}_2$ with ribbon superstructure. To study the cause of this phenomenon, they calculated a series of different structural models through DFT. Robert A.H. et al. [41] found in the honeycomb structure, two O

atoms dimerize and connect to a Mn. This dimerization forms $\text{Mn-}\eta^1\text{-O}_2$, reduces the total energy of charged structures, and promotes the migration of transition metals.

The spinel phase is often regarded as a good cathode material for SIBs because of the stable crystal structure and fast electron transport. However, in practical applications, adjusting the percentage of other structures in the spinel facies complex system is very important. Through DFT calculation, Zhu, et.al. [42] found the proportion of the spinel phase can be controlled by adjusting the formation energy (such as synthesis temperature).

3.2. Ion/Molecular Diffusion Dynamics Simulation

The ion diffusion property of battery material is one of the important properties of battery, which affects the rate of electrochemical reaction inside the battery [43]. As an effective way to study the mechanism of ion conduction, DFT calculation is widely used in the research of sodium-ion cathode materials.

Pandit et al. [44] used DFT to study the effect of sodium on $\alpha\text{-MnO}_2$. Through the first principles DFT calculation, they found $\alpha\text{-MnO}_2$ has high-diffusion kinetics, and the diffusion barrier is 0.21 eV, shown in Table 1. The experimental results showed $\alpha\text{-MnO}_2$ was an ideal cathode material for SIBs. Lee et al. [45] calculated the energy required for the diffusion of Na^+ in $\text{P2-Na}_x[\text{Ni}_{1/3}\text{Mn}_{2/3}]\text{O}_2$ and found that compared with Li^+ analogues, it was only 170 meV ($1/3 < x < 2/3$).

Table 1. Comparison of DFT calculation data and experimental data of some materials.

Material Type	DFT Calculation Purpose	Calculation Results	Experimental Result	Reference
$\alpha\text{-MnO}_2$	lattice parameters	a [\AA]: 9.763 b [\AA]: 9.763 c [\AA]: 2.872	a [\AA]: 9.815 b [\AA]: 9.815 c [\AA]: 2.847	[44]
$\alpha\text{-MnO}_2$	reaction voltages	3.42 V	3.23 V	[44]
$\alpha\text{-MnO}_2$	electronic band	2.42 eV	2.23 eV	[44]
$\beta\text{-NaMnO}_2$	migration energy barrier	0.3 eV	0.27 eV	[46]
$\text{Na}_{3.41}\text{Fe}_{0.59}\text{V}(\text{PO}_4)_3$ (Pristine)	lattice parameters	a [\AA]: 8.9675 c [\AA]: 21.6030 V [\AA^3]: 1504.48	a [\AA]: 8.8818 c [\AA]: 21.5092 V [\AA^3]: 1469.95	[47]
$\text{Na}_{3.41}\text{Fe}_{0.59}\text{V}(\text{PO}_4)_3$ (cutoff voltage at 4.4 V vs. Na + /Na.)	lattice parameters	a [\AA]: 8.5344 c [\AA]: 21.7468 V [\AA^3]: 1371.74	a [\AA]: 8.6726 c [\AA]: 21.789 V [\AA^3]: 1419.3	[47]
$\text{Na}_x\text{V}_2(\text{PO}_4)_3$ ($1 < x < 3$)	reaction voltages	3.4 V	3.3 V	[48]
$\text{Na}_2\text{FePO}_4\text{F}$	band gap energy	2.19 eV	2.80 eV	[49]
$\text{Na}_2\text{Fe}_{0.5}\text{Mn}_{0.5}\text{PO}_4\text{F}$	band gap energy	1.36 eV	1.93 eV	[49]
$\text{Na}_3\text{V}_2(\text{PO}_4)_3$	band gap energy	1.75 eV	4.89 eV	[50]
$\text{Na}_3\text{V}_{1.8}\text{Al}_{0.2}(\text{PO}_4)_3$	band gap energy	1.58 eV	4.64 eV	[50]
$\text{FeMn}(\text{CN})_6$	lattice parameters	a [\AA]: 7.09 b [\AA]: 7.31 c [\AA]: 10.69	a [\AA]: 7.15 b [\AA]: 7.15 c [\AA]: 10.54	[51]
$\text{NaFeMn}(\text{CN})_6$	lattice parameters	a [\AA]: 7.19 b [\AA]: 7.97 c [\AA]: 10.67	a [\AA]: 7.54 b [\AA]: 7.54 c [\AA]: 10.66	[51]
$\text{FeMn}(\text{CN})_6$	lattice parameters	a [\AA]: 6.55 b [\AA]: 6.55 c [\AA]: 19.51	a [\AA]: 6.58 b [\AA]: 6.58 c [\AA]: 18.93	[51]
$\text{FeMn}(\text{CN})_6 \cdot 2\text{H}_2\text{O}$	lattice parameters	a [\AA]: 7.08 b [\AA]: 7.30 c [\AA]: 10.73	a [\AA]: 7.15 b [\AA]: 7.15 c [\AA]: 10.54	[51]
$\text{NaFeMn}(\text{CN})_6 \cdot 2\text{H}_2\text{O}$	lattice parameters	a [\AA]: 7.40 b [\AA]: 7.63 c [\AA]: 10.69	a [\AA]: 7.50 b [\AA]: 7.50 c [\AA]: 10.60	[51]

Table 1. Cont.

Material Type	DFT Calculation Purpose	Calculation Results	Experimental Result	Reference
$\text{Na}_2\text{FeMn}(\text{CN})_6 \cdot 2\text{H}_2\text{O}$	lattice parameters	a [Å]: 7.39 b [Å]: 7.47 c [Å]: 10.61	a [Å]: 7.34 b [Å]: 7.53 c [Å]: 10.59	[51]
$\text{Na}_2\text{Fe}[\text{Fe}(\text{CN})_6]$	lattice parameters	a [Å]: 10.302 b [Å]: 10.302 c [Å]: 10.302	a [Å]: 10.259 b [Å]: 10.259 c [Å]: 10.259	[52]
$\text{NaFe}[\text{Fe}(\text{CN})_6]$	lattice parameters	a [Å]: 10.244 b [Å]: 10.244 c [Å]: 10.244	a [Å]: 10.194 b [Å]: 10.194 c [Å]: 10.194	[52]
$\text{Na}_2\text{Fe}[\text{Fe}(\text{CN})_6]$	reaction voltages	3.32 V	3.23 V	[52]
C-NiHCF	lattice parameters	a [Å]: 10.143 b [Å]: 10.143 c [Å]: 10.143	a [Å]: 10.227 b [Å]: 10.227 c [Å]: 10.227	[53]
M-NiHCF	lattice parameters	a [Å]: 10.617 b [Å]: 7.601 c [Å]: 7.398	a [Å]: 10.361 b [Å]: 7.417 c [Å]: 7.219	[53]
$\text{Na}_2\text{C}_6\text{H}_2\text{O}_4$	reaction voltages	1.17 V	1.21 V	[54]
$\text{Na}_3\text{C}_6\text{H}_2\text{O}_4$	reaction voltages	0.95 V	1.31 V	[54]
$\text{Na}_4\text{C}_6\text{H}_2\text{O}_4$	reaction voltages	1.38 V	1.49 V	[54]
polyaniline (PANI) and cyano (CN) functionalized	increased voltage	0.7–1.1 V	1.3 V	[55]

Sodium ions have different diffusion kinetics in P2 and O3 phase structures. It is generally believed this is due to the difference in phase structure because the migration path of Na^+ in the O3 phase structure is longer than that in the P2 phase. To test this view, Rojo et al. [56] synthesized O3 and P2 phase $\text{Na}_{2/3}\text{Fe}_{2/3}\text{Mn}_{1/3}\text{O}_2$ with the same stoichiometry and used the DFT calculation to study the diffusion of Na^+ in them. Through calculation and comparison, they found Na^+ diffusion resistance of the P2 phase was still lower than that of the O3 phase after excluding factors, such as sodium-ion content and the oxidation state of transition metals. This also proves the diffusion ability of sodium ions in two phases is mainly related to the structure.

Carbon-coated metal chalcogenide composites often show better electrochemical performance. Zhai et al. [57] found composite $\text{Fe}_x\text{Se}_y@\text{CN}$ has higher Na^+ ion diffusion coefficient than pure Fe_xSe_y through calculation. They thought the Ni-doped carbon layer coated on the surface of the Fe_xSe_y micro rod may be the reason for accelerating charge transfer and Na^+ ion diffusion.

3.3. Analysis of Electronic Structure

The calculation of electronic structure of electrode materials can reflect the stability of materials, electron transfer, and atomic bonding. By analyzing the electronic structure, we can obtain the density of electronic states, and then we can find the energy band gap of materials and judge the orbital occupation of valence electrons in different transition metals. The DFT calculation can theoretically judge whether the battery design is reasonable by calculating the energy level of the electrode material.

According to the energy band theory of solid-state physics, the electronic conductivity of electrode materials will increase with the decrease of band gap. In sodium-ion cathode materials, people often reduce the band gap by doping. When Jiang et al. [46] studied the $\beta\text{-NaMnO}_2$ layered material, they used the method of Cu doping to improve its electronic conductivity. Through the DFT calculation, they found the band gap of the material decreased from 0.7 eV before doping to 0.3 eV, shown in Table 1, which indicates Cu doping helps to improve the electronic conductivity of $\beta\text{-NaMnO}_2$ material.

The original layer of anion redox in the $\text{P2-Na}_{0.67}\text{Ni}_{0.33}\text{Mn}_{0.67}\text{O}_2$ electrode was once unknown. Zuo et al. [58] combined X-ray absorption spectra and DFT calculations to confirm the oxygen redox in $\text{Na}_{0.67}\text{Ni}_{0.33}\text{Mn}_{0.67}\text{O}_2$ originates from the Ni-O antibonding state. Additionally, when the sodium content is very low, the charge redistribution process between the Ni and O ions is very likely to occur. This has deepened the understanding of this material.

To overcome the capacity loss of the system caused by the strong Jahn–Teller distortion of Mn^{3+} in layered Na_xMnO_2 cathode materials and the capacity loss caused by the irreversible structure evolution of Na_xNiO_2 cathode materials during the charge discharge cycle, [59–61] Lee [45] integrated these two systems into Ni/Mn based layered transition metal oxides (LTMOs), $\text{P2-Na}_x[\text{Ni}_{1/3}\text{Mn}_{2/3}]\text{O}_2$. Through the calculation of the density of states (DOS), they found the three-dimensional orbits of Ni and Mn ions experienced different electronic transitions in which Mn ions remained in the tetravalent state during the Na^+ extraction process, making the Jahn–Teller distortion difficult to produce. Thus, Ni/Mn based-LTMOs have higher specific capacity and more stable structure.

4. Application of DFT Calculation in Polyanionic Compounds

Sodium-based polyanionic compounds are compounds with three-dimensional network structures formed by the strong covalent bond connection of polyanion polyhedron and transition metal ion polyhedron. It has an open three-dimensional skeleton, good magnification performance, and good cycle performance. This section introduces the latest application of the DFT calculation in the polyanion cathode.

4.1. Energy Calculation and Structural Stability Judgment

Before designing new electrode materials, the DFT calculation is often used to predict the feasibility of new material preparation. Wang et al. [62] used the DFT calculation to compare a series of $\text{Na}_x\text{MnM}(\text{PO}_4)_3$ cathodes. After comparison, they successfully synthesized $\text{Na}_4\text{MnCr}(\text{PO}_4)_3$. It is estimated the average voltage provided by $\text{Na}_4\text{MnCr}(\text{PO}_4)_3$ is about 4 V. To find the lowest energy structure of a new NASICON material, $\text{Na}_{3.41}\text{Fe}_{0.59}\text{V}(\text{PO}_4)_3$, in its original state and charged state, Mohammed et al. [47] determined the five most favorable original state structures and the eight most favorable charged state structures through coulomb energy analysis. Then, they used their DFT calculations, respectively, and finally obtained the structure with the lowest total energy. Jian et al. [48] also calculated the voltage curve of $\text{Na}_x\text{V}_2(\text{PO}_4)_3$ before the experiment and found when x is between 1 and 3, the calculated voltage is 3.4 V, but when x is between 3 and 4, the calculated voltage is quite different from the experimental result, shown in Table 1.

Kim et al. [63] used DFT to prove the Na1 site in $\text{Na}_3\text{V}(\text{PO}_3)_3\text{N}$ has higher site energy than the other two sites, which is the reason why the volume change is only 0.16% when it changes from its initial state to $\text{Na}_2\text{V}(\text{PO}_3)_3\text{N}$. Ling et al. [64] used the DFT calculation to calculate the free energy of $\text{Na}_3\text{Zr}_2(\text{SiO}_4)_2(\text{PO}_4)$ and Ge doped $\text{Na}_3\text{Zr}_{1.875}\text{Ge}_{0.125}\text{Si}_2\text{PO}_{12}$ materials in the rhombohedral and monoclinic phases, respectively. They found before Ge doping, the free energies of the two phases had little difference, but after Ge doping, the energy difference of the two phases reached 13 kJ mol^{-1} , and the rhombohedral phase was more stable, and the conductivity of the material was also improved.

4.2. Ion/Molecular Diffusion Dynamics Simulation

Ion doping is usually used as a good means to improve the electrochemical performance of cathode materials. Li et al. [65] proposed the modification of Mn^{2+} doped $\text{Na}_4\text{Fe}_3(\text{PO}_4)_2\text{P}_2\text{O}_7$ (NFPP) and graphene. Through the DFT calculation, they found Mn^{2+} doping can effectively reduce the energy barrier of the material, thus improving its conductivity. Chen et al. [66] prepared NASICON type $\text{Na}_3\text{V}_{1.5}\text{Al}_{0.5}(\text{PO}_4)_3$ sodium-ion cathode by the sol-gel method. According to the DFT calculation, they found NASICON's three-

dimensional sodium-ion diffusion path has a low Na^+ diffusion barrier, and its structural stability is improved by Al^{3+} substitution.

Wang et al. [39] synthesized a new NASICON-related structure, $\text{Na}_4\text{MnAl}(\text{PO}_4)_3$. With the first principles calculation, they studied the storage and diffusion mechanism of sodium ions and revealed the low-barrier diffusion path along $\text{Na}(1) \leftrightarrow \text{Na}(2) \leftrightarrow \text{Na}(3)$ in $\text{Na}_4\text{MnAl}(\text{PO}_4)_3$ for the first time through the DFT calculation, shown in Figure 2c–h, indicating it has dynamic advantages as an SIBs cathode material. Song et al. [67] studied the ion migration behavior of $\text{Na}_3\text{V}_2(\text{PO}_4)_3$ with the DFT calculation; they found the Na2 site was more active and mainly migrated along three paths with energy of 0.0904, 0.11774, and 2.438 eV, respectively.

Chen et al. [68] measured and analyzed the high-sodium diffusion coefficient of the NASICON type adjustable $\text{Na}_4\text{Fe}_3(\text{PO}_4)_2(\text{P}_2\text{O}_7)/\text{C}$ through the DFT calculation and found all the energy barriers of Na^+ diffusion were lower than 0.9 eV. These lower energy barriers provide a channel for the diffusion of ions in the crystal. This discovery provides strong evidence for the 3D diffusion path of $\text{Na}_4\text{Fe}_3(\text{PO}_4)_2(\text{P}_2\text{O}_7)/\text{C}$ material with NASICON type structure.

4.3. Analysis of Electronic Structure

For the first time, Wei et al. [69] synthesized NaVSi_2O_6 cathode material by the simple sol-gel method. Combined with DFT, they calculated the formation energy changes of Na^+ insertion with different contents and determined the structural changes of the material during charging and discharging by using the volume changes. Thus, the mechanism of NaVSi_2O_6 cycle stability was clarified.

Z.El Kacemi et al. [49] used DFT to study the structure and electrochemical properties of origin and manganese doped $\text{Na}_2\text{FePO}_4\text{F}$. They found through Mn doping 50% of the Fe site in the $\text{Na}_2\text{FePO}_4\text{F}$ lattice, the energy band energy decreased from 2.19 eV to 1.36 eV. Li et al. [70] through the DFT calculation found N-doping in $\text{Na}_3\text{V}_2(\text{PO}_4)_2\text{F}_{2.5}\text{O}_{0.5}$ can significantly reduce the energy gap of the material and significantly improve the conductivity. Zhao et al. [50] studied the effect of Al doping on the electronic structure of $\text{Na}_3\text{V}_2(\text{PO}_4)_3$. It was found the energy band gap in $\text{Na}_3\text{V}_2(\text{PO}_4)_3$ decreased after V was replaced by Al, and the electronic structure changed from indirect band gap to direct band gap, thus improving the electronic conductivity.

With the continuous optimization of the DFT calculation model and the improvement of computer-computing capability, the DFT calculation will be closer to the actual experimental results and can explain the mechanism more deeply, which will bring convenience to research of high specific energy polyanionic compounds cathode materials.

5. Application of DFT Calculation in Prussian Blue

Prussian blue (PB) materials are new cathode materials with great potential developed in recent years. They have an open three-dimensional channel (frame structure), allowing sodium ions to migrate rapidly in the channel so they have good structural stability. This section mainly introduces the latest application of the DFT calculation in PB materials.

5.1. Energy Calculation and Structural Stability Judgment

The formation mechanism of some Prussian blue materials has always been the focus of research. Zuo et al. [71] demonstrated a directional self-assembly strategy to synthesize $\text{Na}_2\text{FeFe}(\text{CN})_6$ material with a three-dimensional flower-like structure. To explore the specific reasons for the formation of these flower-like structures, they calculated the surface adsorption energy of $\text{C}_2\text{H}_5\text{OH}$ material using the DFT method. According to the results of calculation and simulation, they found the OH groups in the material are more inclined to adsorb on the edge and vertex of the crystal, which makes it difficult for the crystal core to grow at these positions, thus making the PB material to present a flower-like structure. To explore the role of Na^+ ions in the structural evolution of NaMnHCF when they are introduced, through DFT calculation, Xiao et al. [51] found when sodium is added, the

increase of Na^+ makes the coulomb gravity of Na-N increase, thus reducing the distance between them and forming a rhombohedral lattice with less distortion.

Kevin Hurlbutt et al. [72] used DFT to calculate the formation energies of various oxidation states and magnetic phases in the $\text{Na}_x\text{Mn}[\text{Mn}(\text{CN})_6]$ system. They found the high specific volume of $\text{Na}_x\text{Mn}[\text{Mn}(\text{CN})_6]$ came from the insertion of the third sodium ion into the molecular formula unit to form $\text{Na}_3\text{Mn}[\text{Mn}(\text{CN})_6]$.

When Shao et al. [73] studied the performance of the PB analog $\text{Na}_2\text{Zn}_3[\text{Fe}(\text{CN})_6]_2$ cathode, they found its solvation energy can be affected by electrolyte concentration. The DFT calculation showed the solvation free energy of $\text{Fe}(\text{CN})_6^{4-}$ increases significantly when using a high-concentration electrolyte. The chemical dissolution of $\text{Na}_2\text{Zn}_3[\text{Fe}(\text{CN})_6]_2$ will become difficult with the increase of solvation free energy.

5.2. Ion/Molecular Diffusion Dynamics Simulation

When comparing the sodium storage kinetics of FeHCF material and a boundary-rich FeHCF material (BR-FeHCF), Huang et al. [74] used the DFT calculation to simulate the insertion process of Na. They calculated the energy change ($\Delta E_{\text{sodiation}}$) and the formula is as follows:

$$\Delta E_{\text{sodiation}} = E_{\text{sodiated PB}} - (E_{\text{PB}} + E_{\text{NA}}) \quad (6)$$

where $E_{\text{sodiated PB}}$, E_{PB} , and E_{NA} represent the total energy of sodium PB, bulk PB, and sodium ions, respectively. It is calculated that the average energy barriers ($\Delta E_{\text{sodiation}}$) of the unit cell in which a sodium ion is inserted into FeHCF and BR-FeHCF are 4.757 and 1.152 eV, respectively, indicating sodium ions can enter the latter more easily and effectively.

Peng et al. [75] used an additive-free “ice-assisted” method to prepare I-PB material with high crystallinity. To further study the storage and transport mechanism of sodium ions in the material, they used the DFT calculation and found the energy barrier of Na^+ migration along the s-shaped path is only 0.11 eV, which is much lower than the 2.81 eV of the defect-rich crystal structure. This makes I-PB as a potential cathode material candidate.

You et al. [76] used the DFT calculation to study the diffusion path of Na^+ in $\text{Na}_x\text{FeFe}(\text{CN})_6$. After investigating four Na^+ diffusion paths, they found the w-type path at the center of the detour has the lowest energy barrier for single Na^+ ion diffusion, which is only 0.58 eV. In the case of Na^+ co-migration, the migration barrier of Na^+ collective migration one by one is the lowest, which is 0.28 eV. It indicates Na^+ is more inclined to co-migrate step by step.

5.3. Analysis of Electronic Structure

Sometimes, when DFT is directly used to describe the electronic properties of transition metals, the calculated results are often inconsistent with the actual situation, which requires improvement of the initial DFT method. The research of Wojde et al. [77,78] shows the DFT+U (Hubbard U) calculation can well predict the structure and electronic properties of electrode materials, such as PB compounds. When Nasir et al. [52] studied $\text{Fe}[\text{Fe}(\text{CN})_6]$ material, they used the DFT+U method and found its description of the electronic properties of sodium ions in PB (shown in Figure 3a) was very similar to the actual situation.

Xu et al. [53] synthesized NiHCF-3 by a simple coprecipitation method. It shows high specific capacity and excellent rate capability of 85.7 mAh g^{-1} . The electronic structure study calculated by DFT (as shown in Figure 3b) reveals the distortion of the NiHCF-3 skeleton leads to the narrowing of the electronic band gap, which promotes the redox activity of Fe, thus producing a monoclinic phase performance with ultra-high velocity and improving the conductivity of NiHCF-3.

Two years later, Xu’s team [79] also used the pyrophosphate-assisted coprecipitation method to synthesize Prussian blue analogs (PBAs) CuHCF nano sheets (CuHCF-P) with high crystallinity and low-water content. They studied the electronic states of these materials through the first principles, shown in Figure 3c,d, and found the main reason for the electrochemical deactivation of Cu/Fe redox centers in CuHCF was there were more initial coordination water molecules, which led to the reduction of the occupied sites of Fe/Cu

three-dimensional orbits and inhibited the charge transfer of two transition metals. In the end, the specific capacity decreases, and cycle stability becomes worse.

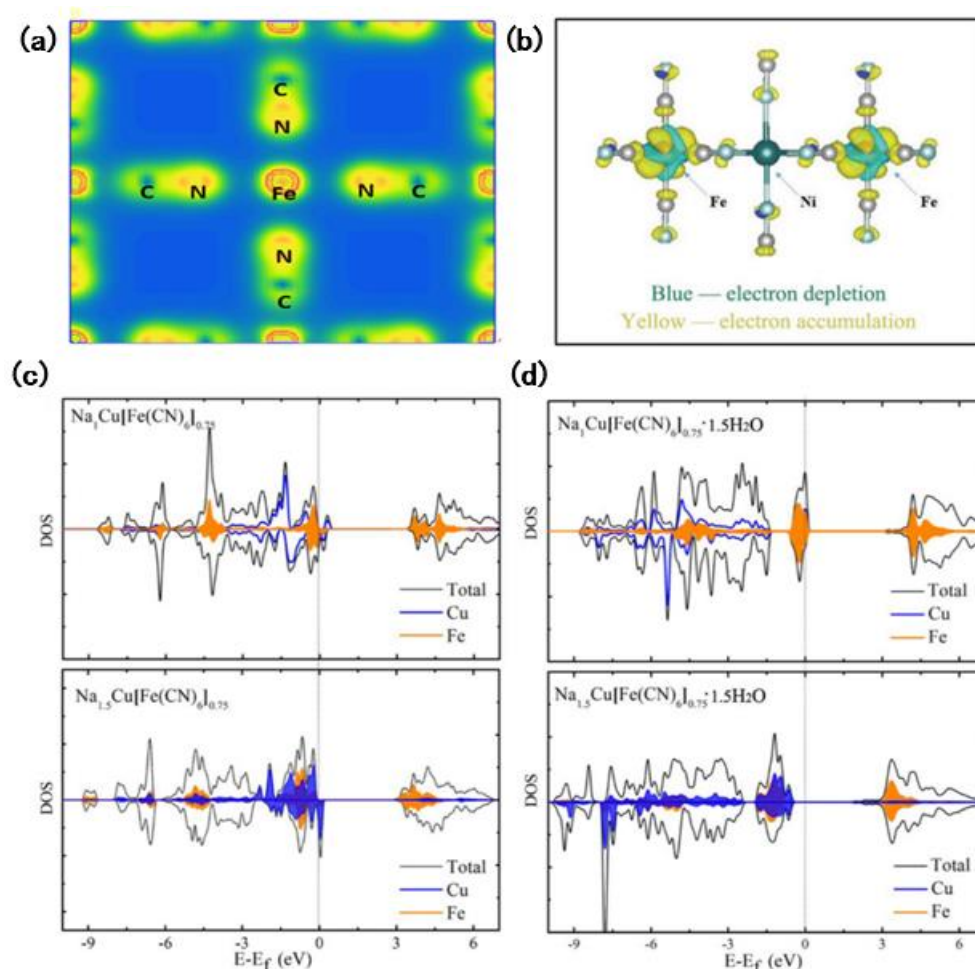


Figure 3. (a) Charge-density diagram of $\text{Fe}[\text{Fe}(\text{CN})_6]$. Reprinted (adapted) with permission from Ref. [52]. Copyright 2019, Informa UK Limited, trading as Taylor & Taylor & Francis Group. (b) Geometry optimized structure of monoclinic NiHCF. Reprinted (adapted) with permission from Ref. [53] Copyright 2021, Elsevier. (c) The charge density difference with an identical distortion and (d) hydrate $\text{Na}_2\text{Cu}[\text{Fe}(\text{CN})_6]_{0.75} \cdot 1.5\text{H}_2\text{O}$ at different Na concentrations, including Na-1 and Na-1.5. Reprinted (adapted) with permission from Ref. [79]. Copyright 2020, Elsevier.

6. Application of DFT Calculation in Organic Materials

Organic compound cathode materials have many advantages, such as rich resources, diverse structures, high sustainability, and environmental friendliness, which are important in the development direction of secondary battery electrode materials. This section introduces the latest application of the DFT calculation in organic materials.

6.1. Energy Calculation and Structural Stability Judgment

Metal organic polymers (MOPs) are considered as potential energy storage materials due to their electrochemical behaviors, such as multi electron reaction, rapid ion diffusion, and small volume change during charging and discharging. [80] Kim et al. [81] firstly introduced aluminum-coordinated poly (P(THBQ-Al)) into sodium-ion batteries as the cathode. Through calculation, they found the electrochemical aluminum cation (Al^{3+}) improved the structural stability of the material during the cycle so that P(THBQ-Al) has a stable structure and performance.

To understand the Na^+ storage mechanism of ultrathin quinone-rich polydopamine (PDA) coating, which is tightly adhered on the 3D porous carbon surface (PC-PDA-APS), Huangfu et al. [82] used the DFT method to calculate its structure and corresponding energy distribution. They found compared with the unsubstituted PDA, the binding energy of Na^+ gradually inserted into the C=O group decreased significantly (-2.97 eV and -1.72 eV), indicating Na^+ has a stable carbonyl-binding tendency in PDA. Zhou et al. [83] designed a novel composite nanofibrous organic cathode consisting of perylenetetracarboxylic dianhydride /nitrogen-doped carbon/carbon nanotubes (PTCDA/NC/CNT) for SIBs. They measured the surface charge of PTCDA/NC/CNT nanofibers at different electrolyte concentrations and used the DFT model to calculate the pore width distribution.

6.2. Ion/Molecular Diffusion Dynamics Simulation

The diffusion of sodium ions in organic materials has always been a research hotspot. Wu et al. [54] studied the diffusion trajectory of Na^+ ions in the original structure of organic material $\text{Na}_2\text{C}_6\text{H}_2\text{O}_4$ and the $\text{Na}_4\text{C}_6\text{H}_2\text{O}_4$ structure embedded in sodium through DFT. They found sodium ions formed obvious two-dimensional channels. At the temperature of 1200 K, the mean square displacement of C, H, and O in the two structures is very small, but the mean square displacement of sodium ions is large, which indicates the benzene ring frame in the two structures is relatively stable, and only sodium ions can diffuse.

Wang et al. [84] synthesized a metal-organic polymer Ni coordination tetraaminobenzoquinone (Ni-TABQ). Through calculation, they found Na^+ can diffuse rapidly along the chain direction in Na_2 Ni-TABQ. After embedding two Na^+ in the Na_4 Ni-TABQ structure, Na^+ can not only spread rapidly along the chain direction but also spread across the chain with a lower diffusion barrier. This unique two-dimensional Na^+ diffusion channel and rapid Na^+ diffusion kinetics provide a basis for its use as a very competitive electrode material for SIBs.

6.3. Analysis of Electronic Structure

To study and reveal the storage mechanism of organic carbonyl compounds, Wu et al. [54] observed the local structure of the organic material, $\text{Na}_2\text{C}_6\text{H}_2\text{O}_4$, before and after sodium insertion and calculated the electronic number of each atom and its change before and after sodium insertion through DFT. They found the number of electrons obtained by the carbon atom on the benzene ring after sodium insertion is more than that of the oxygen atom. This discovery indicates in the crystal state of the organic material, the redox center is the benzene ring, not the carbon oxygen double bond.

How to expand the capacity of organic compound electrode materials has always been a topic of concern for researchers. Xiong et al. [85] synthesized an organic compound, P5Q, through the hybridization of organic compounds and studied its band gap through the DFT calculation. After calculation, they found the energy gap of P5Q is 3.43 eV. This result showed the capacity of hybrid compounds has been significantly improved.

Chen et al. [55] used the combination of molecular dynamics and DFT to calculate the oxidation process of the coordination of polyaniline (PANI) and cyano- (CN) functionalized PANI with electrolyte anions and found the voltage increased by about 0.7–1.1 V through cyano functionalization, shown in Table 1.

7. Outlook and Personal Perspectives

In this paper, we summarized the application of DFT in the cathode materials of sodium-ion batteries and took several experimental cases as examples to illustrate the importance of the DFT calculation in the research of cathode materials. In general, the future applications of DFT computing include the following aspects:

1. DFT calculation can effectively predict the electronic structure of materials, such as the highest occupied molecular orbital, the lowest unoccupied energy level orbital, band gap, etc. Thus, it can predict the physical and chemical properties of various

- molecules and nanoparticles of the cathode materials of sodium-ion batteries, greatly accelerating the identification, characterization, and optimization of materials.
2. The electron transport properties can be predicted by combining with DFT, which can effectively predict the transport and diffusion of sodium ions in materials, thus predicting their sodium-ion conductivity.
 3. Based on the existing material database, the stability of the sodium-ion battery can be predicted. Therefore, the feasibility prediction is carried out before the experiment, which greatly saves the time and costs of the experiment and has guiding significance for the experimental process.
 4. The combined DFT calculation with relevant characterization techniques were taken as a supplement and extension of experimental disciplines to better understand the structure–activity relationship between material structure and performance; it can provide a scientific theoretical basis for the development and design of cathode materials for sodium-ion batteries.

With the development of computer technology, the application of first principles computing simulation will be more and more extensive in the future. The relationship between the structure and performance of the battery material will be better understood by analyzing the specific working principle of battery material through theoretical calculation and combining with high-precision experimental characterization technology. Selecting materials with good performance from a large number of electrode materials through theoretical calculation can avoid unnecessary complex experiments and instrument characterization. We believe using theoretical calculations to guide experiments can often save time and costs and will make greater contributions to the development of electrode materials.

Author Contributions: Conceptualization, Y.W.; writing—original draft preparation, Y.W.; writing—review and editing, Y.W., B.Y., J.X. and M.C.; supervision, M.C. and L.Z.; funding acquisition, M.C. and L.Z. All authors have read and agreed to the published version of the manuscript.

Funding: This research was supported by the Natural Science Foundation of China (Grants No. 52202254), the Natural Science Foundation of Jiangsu Province (Grants No. BK 20220966), and the Fundamental Research Funds for the Central Universities”, No. 30922010708. This research was also supported by the High-End Foreign Experts Project, No. G2022182008L.

Data Availability Statement: No new data were created or analyzed in this study. Data sharing is not applicable to this article.

Conflicts of Interest: The authors declare no conflict of interest.

References

1. Dunn, B.; Kamath, H.; Tarascon, J.M. Electrical energy storage for the grid: A battery of choices. *Science* **2011**, *334*, 928–935. [[CrossRef](#)] [[PubMed](#)]
2. Lu, Y.X.; Zhao, C.L.; Rong, X.H.; Chen, L.Q.; Hu, Y.S. Research progress of materials and devices for room-temperature Na-ion batteries. *Acta Phys. Sin.* **2018**, *67*, 120601.
3. Delmas, C. Sodium and Sodium-Ion Batteries: 50 Years of Research. *Adv. Energy Mater.* **2018**, *8*, 1703137. [[CrossRef](#)]
4. Pan, H.L.; Hu, Y.S.; Chen, L.Q. Room-temperature stationary sodium-ion batteries for large-scale electric energy storage. *Energy Environ. Sci.* **2013**, *6*, 2338–2360. [[CrossRef](#)]
5. Kubota, K.; Komaba, S. Review-Practical Issues and Future Perspective for Na-Ion Batteries. *J. Electrochem. Soc.* **2015**, *162*, A2538–A2550. [[CrossRef](#)]
6. Palomares, V.; Casas-Cabanas, M.; Castillo-Martinez, E.; Han, M.H.; Rojo, T. Update on Na-based battery materials. A growing research path. *Energy Environ. Sci.* **2013**, *6*, 2312–2337. [[CrossRef](#)]
7. Coetzer, J. A new high-energy density battery system. *J. Power Sources* **1986**, *18*, 377–380. [[CrossRef](#)]
8. Okada, S.; Takahashi, Y.; Kiyabu, T. *210th ECS Meeting Abstracts*; MA2006-02; Electrochemical Society (ECS): Pennington, NJ, USA, 2006.
9. Winter, M.; Barnett, B.; Xu, K. Before Li ion batteries. *Chem. Rev.* **2018**, *118*, 11433–11456. [[CrossRef](#)]
10. Li, L.L.; Yu, D.S.; Li, P.; Huang, H.J.; Xie, D.Y.; Lin, C.C.; Hu, F.; Chen, H.Y.; Peng, S.J. Interfacial electronic coupling of ultrathin transition-metal hydroxide nanosheets with layered MXenes as a new prototype for platinum-like hydrogen evolution. *Energy Environ. Sci.* **2021**, *14*, 6419–6427. [[CrossRef](#)]

11. Xu, S.; Wu, X.; Li, Y. Novel copper redox-based cathode materials for room-temperature sodium-ion batteries. *Chin. Phys. B* **2014**, *23*, 118202. [[CrossRef](#)]
12. Shacklette, L.W.; Jow, T.R.; Townsend, L. Rechargeable electrodes from sodium cobalt bromzes. *J. Electrochem. Soc.* **1988**, *135*, 2669–2674. [[CrossRef](#)]
13. Asl, H.Y.; Manthiram, A. Reining in dissolved transition-metal ions. *Science* **2020**, *369*, 140–141. [[CrossRef](#)] [[PubMed](#)]
14. Kresse, G.; Furthmüller, J. Efficiency of ab-initio total energy calculations for metals and semiconductors using a plane-wave basis set. *Phys. Rev. B* **1996**, *54*, 11169–11186. [[CrossRef](#)]
15. Payne, M.C.; Teter, M.P.; Allan, D.C. Iterative minimization techniques for ab initio total-energy calculations-molecular-dynamics and conjugate gradients. *Rev. Mod. Phys.* **1992**, *64*, 1045–1097. [[CrossRef](#)]
16. Alder, B.J.; Wainwright, T.E. Studies in molecular dynamics. I. General Method. *J. Chem. Phys.* **1959**, *31*, 459–466. [[CrossRef](#)]
17. Car, R.; Parrinello, M. Unified approach for molecular dynamics and density-functional theory. *Phys. Rev. Lett.* **1985**, *55*, 2471–2474. [[CrossRef](#)] [[PubMed](#)]
18. Ong, S.P.; Chevrier, V.L.; Hautier, G.; Jain, A.; Moore, C.; Kim, S.; Ma, X.; Ceder, G. Voltage, stability and diffusion barrier differences between sodium-ion and lithium-ion intercalation materials. *Energy Environ. Sci.* **2011**, *4*, 3680–3688. [[CrossRef](#)]
19. Yang, L.; Chen, R.S.; Liu, Z.P.; Gao, Y.R.; Wang, X.F.; Wang, Z.X.; Chen, L.Q. Configuration-dependent anionic redox in cathode materials. *Battery Energy* **2022**, *1*, 2021001. [[CrossRef](#)]
20. Chevrier, V.L.; Ceder, G. Challenges for Na-ion Negative Electrodes. *J. Electrochem. Soc.* **2011**, *158*, A1011–A1014. [[CrossRef](#)]
21. Mo, Y.; Ong, S.P.; Ceder, G. Insights into Diffusion Mechanisms in P2 Layered Oxide Materials by First-Principles Calculations. *Chem. Mater.* **2014**, *26*, 5208–5214. [[CrossRef](#)]
22. Dacek, S.T.; Richards, W.D.; Kitchaev, D.A. Structure and Dynamics of Fluorophosphate Na-Ion Battery Cathodes. *Chem. Mater.* **2016**, *28*, 5450–5460. [[CrossRef](#)]
23. He, Q.; Yu, B.; Li, Z.H.; Zhao, Y. Density Functional Theory for Battery Materials. *Energy Environ. Mater.* **2019**, *2*, 264–279. [[CrossRef](#)]
24. Zhang, M.; Tong, Y.F.; Xie, J.; Huang, W.W.; Zhang, Q.C. Rechargeable Sodium-Ion Battery Based on Polyazaacene Analogue Anode. *Chem. Eur. J.* **2021**, *27*, 16754–16759. [[CrossRef](#)]
25. Li, J.Y.; Hu, H.Y.; Wang, J.Z.; Xiao, Y. Surface chemistry engineering of layered oxide cathodes for sodium-ion batteries. *Carbon Neutralization* **2022**, *1*, 96–116. [[CrossRef](#)]
26. Volkov, A. *Ionic and Electronic Transportation Electrochemical and Polymer Based Systems*; Linköping University Electronic Press: Linköping, Sweden, 2017.
27. Parr, R.G.; Yang, W. *Density-Functional Theory of Atoms and Molecules*; Oxford University Press: New York, NY, USA, 1989.
28. Dreizler, R.M.; Gross, E.K.U. *Density Functional Theory: An Approach to the Quantum Many Body Problem*; Springer: Berlin/Heidelberg, Germany, 1990.
29. Kryachko, E.S.; Ludena, E.V. *Density Functional Theory of Many Electron Systems*; Kluwer: Dordrecht, The Netherlands, 1990.
30. March, N.H. *Electron Density Theory*; Academic Press: London, UK, 1992.
31. Chong, D.P. *Recent Advances in Density Functional Methods*; World Scientific: Singapore, 1995.
32. Nalewajski, R.F.; Mrozek, J. Hartree-Fock difference approach to chemical valence: Three-electron indices in UHF approximation. *Int. J. Quantum Chem.* **1996**, *57*, 377–389. [[CrossRef](#)]
33. Parr, R.G.; Yang, W. Density-functional theory of the electronic structure of molecules. *Annu. Rev. Phys. Chem.* **1995**, *46*, 701–728. [[CrossRef](#)]
34. Kohn, W.; Sham, L.J. Self-consistent equations including exchange and correlation effects. *Phys. Rev.* **1965**, *140*, A1133–A1138. [[CrossRef](#)]
35. Szalewicz, K. Determination of Structure and Properties of Molecular Crystals from First Principles. *Acc. Chem. Res.* **2014**, *47*, 3266–3274. [[CrossRef](#)]
36. Patkowski, K.; Szalewicz, K. Argon Pair Potential at Basis and Excitation Limits. *J. Chem. Phys.* **2010**, *133*, 094304. [[CrossRef](#)]
37. Jensen, F. *Introduction to Computational Chemistry*, 2nd ed.; Wiley: Chichester, UK, 2007.
38. Toumar, A.J.; Ong, S.P.; Richards, W.D.; Dacek, S.; Ceder, G. Vacancy Ordering in O3 -Type Layered Metal Oxide Sodium-Ion Battery Cathodes. *Phys. Rev. Appl.* **2015**, *4*, 064002. [[CrossRef](#)]
39. Wang, Q.C.; Lin, C.; Li, J.B.; Gao, H.C.; Wang, Z.G.; Jin, H.B. Experimental and theoretical investigation of Na₄MnAl(PO₄)₃ cathode material for sodium-ion batteries. *Chem. Eng. J* **2021**, *425*, 130680. [[CrossRef](#)]
40. Matteo, B.; Wang, J.Y.; Clément, R.; Ceder, G. A First-Principles and Experimental Investigation of Nickel Solubility into the P2 Na_xCoO₂ Sodium-Ion Cathode. *Adv. Energy Mater.* **2018**, *8*, 1801446.
41. House, R.A.; Maitra, U.; Pérez-Osorio, M.A.; Lozano, J.G.; Jin, L.; Somerville, J.W.; Duda, L.C.; Nag, A.; Walters, A.; Zhou, K.J.; et al. Superstructure control of first-cycle voltage hysteresis in oxygen-redox cathodes. *Nature* **2020**, *577*, 502–508. [[CrossRef](#)]
42. Zhu, Y.F.; Xiao, Y.; Dou, S.X.; Kang, Y.M.; Chou, S.L. Spinel engineering on layered oxide cathodes for sodium-ion batteries. *eScience* **2021**, *1*, 13–27. [[CrossRef](#)]
43. Nakayama, M.; Kaneko, M.; Wakihara, M. First-principles study of lithium-ion migration in lithium transition metal oxides with spinel structure. *Phys. Chem. Chem. Phys.* **2012**, *14*, 13963–13970. [[CrossRef](#)]

44. Pandit, B.; Rondiya, S.R.; Dzade, N.Y.; Shaikh, S.F.; Kumar, N.; Goda, E.S.; Al-Kahtani, A.A.; Mane, R.S.; Mathur, S.; Salunkhe, R.R. High Stability and Long Cycle Life of Rechargeable Sodium-Ion Battery Using Manganese Oxide Cathode: A Combined Density Functional Theory (DFT) and Experimental Study. *ACS Appl. Mater. Interfaces* **2021**, *13*, 11433–11441. [[CrossRef](#)]
45. Lee, D.H.; Xu, J.; Meng, Y.S. An advanced cathode for Na-ion batteries with high rate and excellent structural stability. *Phys. Chem. Chem. Phys.* **2013**, *15*, 3304–3312. [[CrossRef](#)]
46. Jiang, L.W.; Lu, Y.X.; Wang, Y.S.; Liu, L.L.; Qi, X.G.; Zhao, C.L.; Chen, L.Q.; Hu, Y.S. A High-Temperature β -Phase NaMnO₂ Stabilized by Cu Doping and Its Na Storage Properties. *Chin. Phys. Lett.* **2018**, *35*, 048801. [[CrossRef](#)]
47. Mohammed, H.; Najma, Y.; Payam, K.; Tan, M.X.; Liu, J.; Sang, P.F.; Fu, Y.Z.; Huang, Y.H.; Ma, J.W. Fast sodium intercalation in Na_{3.41}Fe_{0.59}(PO₄)₃: A novel sodium-deficient NASICON cathode for sodium-ion batteries. *Energy Storage Mater.* **2020**, *35*, 192–202.
48. Jian, Z.L.; Sun, Y.; Ji, X.L. A new low-voltage plateau of Na₃V₂(PO₄)₃ as an anode for Na-ion batteries. *Chem. Commun.* **2015**, *51*, 6381–6383. [[CrossRef](#)]
49. El Kacemi, Z.; Mansouri, Z.; Benyoussef, A.; El Kenz, A.; Balli, M.; Mounkachi, O. First principle calculations on pristine and Mn-doped iron fluorophosphates as sodium-ion battery cathode materials. *Comput. Mater. Sci.* **2022**, *206*, 111292. [[CrossRef](#)]
50. Zhao, L.N.; Zhao, H.L.; Du, Z.H.; Chen, N.; Chang, X.W.; Zhang, Z.J.; Gao, F.; Trenczek-Zajac, A.; Świerczek, K. Computational and experimental understanding of Al-doped Na₃V_{2-x}Al_x(PO₄)₃ cathode material for sodium ion batteries: Electronic structure, ion dynamics and electrochemical properties. *Electrochim. Acta* **2018**, *282*, 510–519. [[CrossRef](#)]
51. Xiao, P.; Song, J.; Wang, L.; Goodenough, J.B.; Henkelman, G. Theoretical Study of the Structural Evolution of a Na₂FeMn(CN)₆ Cathode upon Na Intercalation. *Chem. Mater.* **2015**, *27*, 3763–3768. [[CrossRef](#)]
52. Nasir, N.A.M.; Badrudin, F.W.; Idrus, A.; Sazman, F.N.; Taib, M.F.M.; Yahya, M.Z.A. First-principles study on structural and electronic properties of Prussian blue cathode material for sodium-ion battery. *Mol. Cryst. Liq. Cryst.* **2019**, *693*, 115–122. [[CrossRef](#)]
53. Xu, Y.; Wan, J.; Huang, L.; Ou, M.Y.; Fan, C.Y.; Wei, P.; Peng, J.; Liu, Y.; Qiu, Y.G.; Sun, X.P.; et al. Structure Distortion Induced Monoclinic Nickel Hexacyanoferrate as High-Performance Cathode for Na-Ion Batteries. *Adv. Energy Mater.* **2018**, *9*, 1803158. [[CrossRef](#)]
54. Wu, X.Y.; Jin, S.F.; Zhang, Z.Z.; Jiang, L.W.; Mu, L.Q.; Hu, Y.S.; Li, H.; Chen, X.L.; Armand, M.; Chen, L.Q. Unraveling the storage mechanism in organic carbonyl electrodes for sodium-ion batteries. *Sci. Adv.* **2015**, *1*, e1500330. [[CrossRef](#)]
55. Chen, Y.Q.; Luder, J.; Ng, M.F.; Michael, S.; Sergei, M.G. Polyaniline and CN-functionalized polyaniline as organic cathodes for lithium and sodium ion batteries: A combined molecular dynamics and density functional tight binding study in solid state. *Phys. Chem. Chem. Phys.* **2018**, *20*, 23. [[CrossRef](#)]
56. Katcho, N.A.; Carrasco, J.; Saurel, D.; Gonzalo, E.; Han, M.; Aguesse, F.; Rojo, T. Commercial Prospects of Existing Cathode Materials for Sodium Ion Storage. *Adv. Energy Mater.* **2017**, *7*, 1601477. [[CrossRef](#)]
57. Zhai, L.F.; Yu, J.M.; Yu, J.P.; Xiong, W.W.; Zhang, Q.C. Thermodynamic Transformation of Crystalline Organic Hybrid Iron Selenide to Fe_xSe_y@CN Microrods for Sodium Ion Storage. *ACS Appl. Mater. Interfaces* **2022**, *14*, 49854–49864. [[CrossRef](#)]
58. Zuo, W.H.; Ren, F.C.; Li, Q.H.; Wu, X.H.; Fang, F.; Yu, X.Q.; Li, H.; Yang, Y. Insights of the anionic redox in P2-Na_{0.67}Ni_{0.33}Mn_{0.67}O₂. *Nano Energy* **2020**, *78*, 105285. [[CrossRef](#)]
59. Caballero, A.; Hernán, L.; Morales, J.; Sánchez, L.; Peña, J.S.; Aranda, M.A.G. Synthesis and characterization of high-temperature hexagonal P2-Na_{0.6}MnO₂ and its electrochemical behaviour as cathode in sodium cells. *J. Mater. Chem.* **2002**, *12*, 1142–1147. [[CrossRef](#)]
60. Han, M.H.; Gonzalo, E.; Casas-Cabanas, M.; Rojo, T. Structural evolution and electrochemistry of monoclinic NaNiO₂ upon the first cycling process. *J. Power Sources* **2014**, *258*, 266–271. [[CrossRef](#)]
61. Wang, S.H.; Sun, C.L.; Wang, N.; Zhang, Q.C. Ni- and/or Mn-based Layered Transition Metal Oxides as Cathode Materials for Sodium Ion Batteries: Status, Challenges and Countermeasurements. *J. Mater. Chem. A* **2019**, *7*, 10138–10158. [[CrossRef](#)]
62. Wang, J.Y.; Wang, Y.; Seo, D.H.; Shi, T.; Chen, S.P.; Tian, Y.S.; Haegyeom, K.; Gerbrand, C. High-performance trifunctional electrocatalysts based on FeCo/Co₂P hybrid nanoparticles for Zinc–Air battery and self-powered overall water splitting. *Adv. Energy Mater.* **2020**, *10*, 1903968. [[CrossRef](#)]
63. Kim, J.; Yoon, G.; Lee, H.M.; Hyungsub, K.; Lee, S.; Kang, K. New 4V-Class and Zero-Strain Cathode Material for Na-Ion Batteries. *Chem. Mater.* **2017**, *29*, 7826–7832. [[CrossRef](#)]
64. Ran, L.B.; Ardeshir, B.; Li, M.; Yin, Y.; Baris, D.; Lin, T.G.; Li, M.; Masud, R.; Ian, G.; Wang, L.Z.; et al. Ge co-doping NASICON boosts solid-state sodium ion batteries' performance. *Energy Storage Mater.* **2021**, *40*, 282–291. [[CrossRef](#)]
65. Li, X.Q.; Zhang, Y.; Zhang, B.L.; Qin, K.; Liu, H.M.; Ma, Z.F. Mn-doped Na₄Fe₃(PO₄)₂P₂O₇ facilitating Na⁺ migration at low temperature as a high-performance cathode material of sodium ion batteries. *J. Power Sources* **2022**, *521*, 230922. [[CrossRef](#)]
66. Sun, S.; Zhao, Y.J.; Ni, Q.; Sun, A.; Yuan, X.Y.; Li, J.B.; Jin, H.B. Revealing excess Al³⁺ preinsertion on altering diffusion paths of aluminum vanadate for zinc-ion batteries. *Energy Storage Mater.* **2022**, *52*, 291–298. [[CrossRef](#)]
67. Song, W.X.; Ji, X.B.; Wu, Z.P.; Zhu, Y.R.; Yang, Y.C.; Chen, J.; Jing, M.J.; Li, F.Q.; Banks, C.E. First exploration of Na-ion migration pathways in the NASICON structure Na₃V₂(PO₄)₃. *J. Mater. Chem.* **2014**, *2*, 5358–5362. [[CrossRef](#)]
68. Chen, M.Z.; Hua, W.B.; Xiao, J.; David, C.; Chen, W.H.; Wang, E.H.; Hu, Z.; Gu, Q.F.; Wang, X.L.; Indris, S.; et al. NASICON-type air-stable and all-climate cathode for sodium-ion batteries with low cost and high-power density. *Nat. Commun.* **2019**, *10*, 1480. [[CrossRef](#)]

69. Wei, Y.B.; Zhang, Y.; Huang, Y.D.; Wang, X.C.; Cheng, W.H.; Sun, Y.; Jia, D.Z.; Tang, X.C. Simple synthesis and electrochemical performance of NaVSi_2O_6 as a new sodium-ion cathode material. *Int. J. Energy Res.* **2021**, *45*, 10746–10751. [[CrossRef](#)]
70. Li, W.; Yao, Z.J.; Liu, Y.; Zhang, S.Z.; Wang, X.L.; Xia, X.H.; Gu, C.D.; Tu, J.P. Optimizing quasi-solid-state sodium storage performance of $\text{Na}_3\text{V}_2(\text{PO}_4)_2\text{F}_{2.5}\text{O}_{0.5}$ cathode by structural design plus nitrogen doping. *Chem. Eng. J.* **2022**, *433*, 133557. [[CrossRef](#)]
71. Zuo, D.X.; Wang, C.P.; Han, J.J.; Wu, J.H.; Qiu, H.J.; Zhang, Q.; Lu, Y.; Lin, Y.J.; Liu, X.J. Oriented Formation of a Prussian Blue Nanoflower as a High-Performance Cathode for Sodium Ion Batteries. *ACS Sustain. Chem. Eng.* **2020**, *8*, 16229–16240. [[CrossRef](#)]
72. Hurlbutt, K.; Giustino, F.; Volonakis, G.; Pasta, M. Origin of the High Specific Capacity in Sodium Manganese Hexacyanomanganate. *Chem. Mater.* **2022**, *34*, 4336–4343. [[CrossRef](#)]
73. Shao, M.M.; Wang, B.; Liu, M.C.; Wu, C.; Ke, F.S.; Ai, X.P.; Yang, H.X.; Qian, J.F. A High-Voltage and Cycle Stable Aqueous Rechargeable Na-Ion Battery Based on $\text{Na}_2\text{Zn}_3[\text{Fe}(\text{CN})_6]_2\text{-NaTi}_2(\text{PO}_4)_3$ Intercalation Chemistry. *ACS Appl. Energy Mater.* **2019**, *2*, 5809–5815. [[CrossRef](#)]
74. Huang, Y.X.; Xie, M.; Zhang, J.T.; Wang, Z.H.; Jiang, Y.; Xiao, G.H.; Li, S.J.; Li, L.; Wu, F.; Chen, R.J. A novel border-rich Prussian blue synthesized by inhibitor control as cathode for sodium ion batteries. *Nano Energy* **2017**, *39*, 273–283. [[CrossRef](#)]
75. Peng, J.; Zhang, W.; Hu, Z.; Zhao, L.F.; Wu, C.; Peleckis, G.; Gu, Q.F.; Wang, J.Z.; Liu, H.K.; Dou, S.X.; et al. Ice-Assisted Synthesis of Highly Crystallized Prussian Blue Analogues for All-Climate and Long-Calendar-Life Sodium Ion Batteries. *Nano Lett.* **2022**, *22*, 1302–1310. [[CrossRef](#)]
76. You, Y.; Xin, S.; Hooman; Asl, Y.; Li, W.D.; Wang, P.F.; Guo, Y.G. Subzero-Temperature Cathode for a Sodium-Ion Battery. *Adv. Mater.* **2016**, *28*, 7243–7248. [[CrossRef](#)]
77. Wojdeł, J.C.; Moreira, I.D.R.; Bromley, S.T.; Illas, F. On the prediction of the crystal and electronic structure of mixed-valence materials by periodic density functional calculations: The case of Prussian Blue. *J. Chem. Phys.* **2008**, *128*, 044713. [[CrossRef](#)]
78. Wojdeł, J.C.; Bromley, S.T. Efficient calculation of the structural and electronic properties of mixed valence materials: Application to Prussian Blue analogues. *Chem. Phys. Lett.* **2004**, *397*, 154–159. [[CrossRef](#)]
79. Xu, Y.; Wan, J.; Huang, L.; Ou, M.Y.; Fan, C.Y.; Wei, P.; Peng, J.; Liu, Y.; Qiu, Y.G.; Sun, X.P.; et al. Dual redox-active copper hexacyanoferrate nanosheets as cathode materials for advanced sodium-ion batteries. *Energy Storage Mater.* **2020**, *33*, 432–441. [[CrossRef](#)]
80. Wu, Z.Z.; Xie, J.; Xu, Z.C.J.; Zhang, S.Q.; Zhang, Q.C. Recent Progress in Metal-Organic Polymers as Promising Electrodes for Lithium/Sodium Rechargeable Batteries. *J. Mater. Chem. A* **2019**, *7*, 4259–4290. [[CrossRef](#)]
81. Kim, H.J.; Kim, Y.; Shim, J.; Jung, K.H.; Jung, M.S.; Kim, H.; Lee, J.C.; Lee, K.T. Environmentally Sustainable Aluminum-Coordinated Poly(tetrahydroxybenzoquinone) as a Promising Cathode for Sodium Ion Batteries. *ACS Appl. Mater. Interfaces* **2018**, *10*, 3479–3486. [[CrossRef](#)] [[PubMed](#)]
82. Huangfu, C.; Liu, Z.; Lu, X.L.; Liu, Q.; Wei, T.; Fan, Z.J. Strong oxidation induced quinone-rich dopamine polymerization onto porous carbons as ultrahigh-capacity organic cathode for sodium-ion batteries. *Energy Storage Mater.* **2021**, *43*, 120–129. [[CrossRef](#)]
83. Zhou, G.Y.; Mo, L.L.; Zhou, C.Y.; Wu, Y.; Lai, F.L.; Lv, Y.; Ma, J.M.; Miao, Y.E.; Liu, T.X. Ultra-strong capillarity of bioinspired micro/nanotunnels in organic cathodes enabled high-performance all-organic sodium-ion full batteries. *Chem. Eng. J.* **2021**, *420*, 127597. [[CrossRef](#)]
84. Wang, L.B.; Ni, Y.X.; Hou, X.S.; Chen, L.; Li, F.J.; Chen, J. A two-dimensional metal-organic polymer enabled by robust nickel-nitrogen and hydrogen bonds for exceptional sodium-ion storage. *Angew. Chem. Int. Ed.* **2020**, *59*, 22126–22131. [[CrossRef](#)]
85. Xiong, W.X.; Huang, W.W.; Zhang, M.; Hu, P.D.; Cui, H.M.; Zhang, Q.C. Pillar [5] quinone–Carbon Nanocomposites as High-Capacity Cathodes for Sodium-Ion Batteries. *Chem. Mater.* **2019**, *31*, 8069–8075. [[CrossRef](#)]

Disclaimer/Publisher’s Note: The statements, opinions and data contained in all publications are solely those of the individual author(s) and contributor(s) and not of MDPI and/or the editor(s). MDPI and/or the editor(s) disclaim responsibility for any injury to people or property resulting from any ideas, methods, instructions or products referred to in the content.